

Path integral study of hydrogen and deuterium diffusion in crystalline silicon

Kelsey M. Forsythe and Nancy Makri

Department of Chemistry, University of Illinois, Urbana, Illinois 61801

(Received 18 June 1997; accepted 22 January 1998)

We use classical and quantum mechanical methods to calculate the site-to-site hopping rate of hydrogen impurities in crystalline silicon over a wide range of temperatures. The calculations employ a parameterized version of a potential surface calculated via density functional methods, expanded through quadratic terms about a Cartesian reaction path with a flexible reference. The hopping rate is obtained from the time integral of a flux correlation function which is evaluated using classical molecular dynamics and real-time path integral techniques. The latter are based on the quasiadiabatic propagator discretization and utilize a combination of discrete variable representations and Monte Carlo sampling for the evaluation of the resulting multidimensional integrals. Our results indicate that quantum mechanical tunneling plays a significant role in the diffusion process even above room temperature. In addition, the calculated diffusion rate exhibits a reverse isotope effect in the domain between activated and tunneling dynamics which arises from the zero point energy of the hydrogen atom in the direction perpendicular to the line connecting two stable minima. © 1998 American Institute of Physics. [S0021-9606(98)51616-9]

I. INTRODUCTION

Understanding the behavior of semiconductor materials and the influence of environmental disturbances on their properties is essential for advances in present-day technology and also for the design of molecular-level devices. One such perturbation is the lattice impurity. In particular, whether in the construction or modification of semiconductors hydrogen is often, welcome or not, a visitor to the lattice. The mobility and amphoteric nature of hydrogen and its isotopes make it reactive with donors or acceptors, changing the electrical and optical properties of the semiconductor.

This article focuses on the dynamical aspects of hydrogen impurities in crystalline silicon. Despite its apparent simplicity, hydrogen has been difficult to observe as an isolated impurity in this material. In particular, experimental measurements of its diffusivity show a sizable spread. At high temperatures, experimental data by Van Wieringen and Warmoltz¹ indicated an Arrhenius dependence of the diffusion coefficient corresponding to an apparent activation energy of 0.48 eV, while at lower temperatures deviations from this Arrhenius curve corresponding to rates that are smaller by several orders of magnitude have been observed.²⁻¹⁰ This unusual behavior has been attributed to the switching of the diffusion mechanism to non-nearest-neighbor hops above a characteristic temperature.⁹

A number of electronic structure calculations^{11,12} predict the bond-center (B) site (the midpoint of a stretched Si-Si bond) as the minimum energy position for a hydrogen impurity. This assignment is in harmony with experimental electron paramagnetic resonance (EPR) data.¹³ Insertion of a hydrogen impurity in a silicon bond is accompanied by significant lattice relaxation, where neighboring silicon atoms exhibit displacements of 0.4 Å while nearest neighbors relax by 0.07 Å.¹²

The dynamical nature of hydrogen has proven more elusive, and several different pathways have been suggested.^{8,9,14,15} The calculations of Van de Walle,¹² based on density functional theory, suggest the saddle point lies near the C site (see Fig. 1). Calculated values of the activation barrier vary from 0.17 eV to 0.84 eV.^{11,14} Given such discrepancies it is not surprising little agreement exists regarding the behavior of the diffusivity, especially at lower temperatures.⁹ Most theoretical studies of the hydrogen dynamics have been based on classical trajectory simulations^{8,9,16} and are therefore restricted to high temperatures. Quantum mechanical treatments employing equilibrium path integral calculations of thermodynamic averages and distribution functions¹⁷⁻¹⁹ have concluded that nonclassical effects can be significant at low temperatures. And most recently centroid path integral calculations showed significant thermally assisted tunneling effects below 100 K.²⁰ However, no dynamical calculations of the contribution of quantum mechanical tunneling to the diffusion process of hydrogen have been reported.

In the following we apply Feynman's path integral formalism to the dynamics of hydrogen impurities in crystalline silicon. For this purpose we employ a Cartesian reaction path decomposition of a parameterized potential energy surface¹⁷ about a flexible lattice geometry²¹ to construct a system-bath Hamiltonian, whose dynamics is treated via numerically exact path integral methods. In particular, we utilize the quasiadiabatic propagator path integral scheme developed earlier in our group²²⁻²⁴ to calculate rate constants for hydrogen motion between adjacent stable sites. The results of the calculations are compared to those predicted via classical rate theories and discussed in connection with experiments and simulations performed on related systems. Our analysis implies significant tunneling contributions for both hydrogen

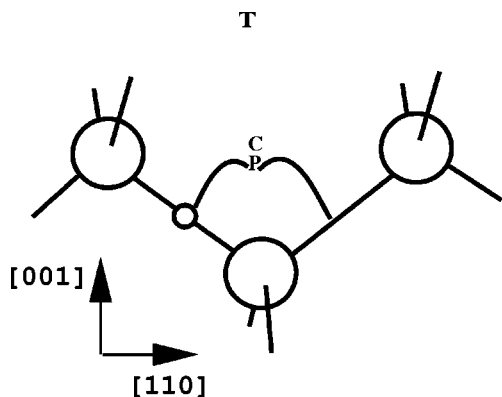


FIG. 1. Silicon lattice atoms surrounding a hydrogen impurity at a stable (B) site. The C and P sites are also shown, along with a sketch of the reaction path.

and deuterium in crystalline silicon, as well as a weak inverse isotope effect originating from the zero point energy in the direction orthogonal to the line connecting two stable sites of the parameterized potential.

Section II describes the potential energy surface that we use and the system-bath decomposition. The path integral methodology is reviewed in Sec. III. Section IV presents the classical and quantum mechanical simulation results for the diffusion rates of hydrogen and deuterium in silicon and discusses the unusual isotope effect that we observe. Some concluding remarks are given in Sec. V.

II. POTENTIAL ENERGY SURFACE AND SYSTEM-BATH DECOMPOSITION

Our calculations employ a single impurity atom embedded within a 64-atom silicon lattice with periodic boundary conditions. This configuration of crystalline silicon has adequately reproduced the experimental phonon spectrum. We adopt a Cartesian coordinate system where the x direction is defined by the line connecting two silicon atoms in the (110) direction and the z coordinate corresponds to the (001) direction.

Herrero and Ramirez have proposed¹⁷ a convenient parameterization of the potential energy surface obtained by Van de Walle using density functional theory.¹² Figure 2(a) shows the parameterized potential energy surface as a function of the x and z coordinates of the hydrogen atom with the lattice atoms relaxed to their equilibrium position at each fixed location of the hydrogen atom. Conjugate gradient minimization was used to generate these surfaces.²⁵ One observes a potential valley that connects the two stable B sites. The midpoint along this valley is a shallow minimum and two saddle points located on either side of this minimum can be identified. We refer to the former midpoint in the metastable region of the potential as the P site. For comparison, the potential surface calculated by Van de Walle has a single saddle point halfway between the two stable sites and somewhat closer to the T site. Contour plots of the parameterized potential surface are also shown in Figs. 2(b) and 2(c) as functions of the x and z coordinates of hydrogen with the lattice atoms fixed at their equilibrium position corresponding to the hydrogen occupying a stable B site and the P site,

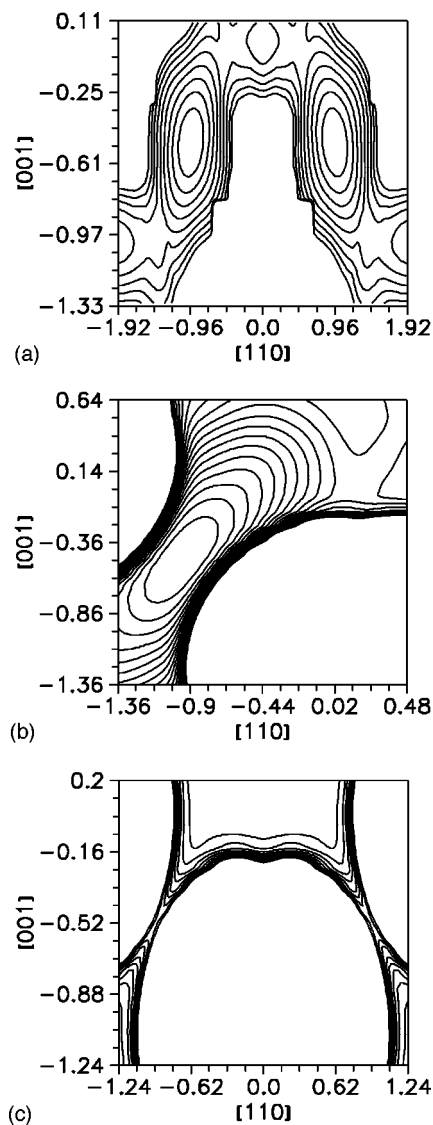


FIG. 2. The parameterized potential surface in the (001) and (110) directions; the unit is angstroms. (a) Silicon lattice atoms relaxed at each position of the hydrogen atom. (b) Lattice relaxed with respect to the hydrogen fixed at a B site. (c) Lattice relaxed with respect to the hydrogen fixed at a P site.

respectively. Note that the unrelaxed B site is not a potential minimum. Indeed, lattice relaxation is quite significant, amounting to a 0.3 Å displacement of the silicon atoms adjacent to hydrogen as the latter is inserted in a B site.

To arrive at a Hamiltonian convenient for calculating diffusion rates we employ a Cartesian reaction path decomposition in which the coordinates of the silicon atoms along with the y coordinate of the hydrogen atom are treated as harmonic degrees of freedom and denoted collectively by \mathbf{R} . The hydrogen-silicon potential is expanded through second order in these coordinates. Due to the sizable relaxation of the silicon lattice, a quadratic expansion about a single equilibrium geometry does not offer an adequate description of the process. Instead, we employ the flexible bath reference developed by Ruf and Miller²¹ where the potential expansion is about a reference configuration $\mathbf{R}_0(\mathbf{r})$ that depends parametrically on the remaining coordinates $r \equiv (x_H, z_H)$ of the hydrogen atom:

$$\begin{aligned}
 V(\mathbf{r}, \mathbf{R}) \approx & V(\mathbf{r}, \mathbf{R}_0(\mathbf{r})) + \left. \frac{\partial V(\mathbf{r}, \mathbf{R})}{\partial \mathbf{R}} \right|_{\mathbf{R}_0(\mathbf{r})} \cdot (\mathbf{R} - \mathbf{R}_0(\mathbf{r})) \\
 & + \frac{1}{2} (\mathbf{R} - \mathbf{R}_0(\mathbf{r})) \cdot \left. \frac{\partial^2 V(\mathbf{r}, \mathbf{R})}{\partial \mathbf{R} \partial \mathbf{R}'} \right|_{\mathbf{R}_0(\mathbf{r})} \cdot (\mathbf{R} - \mathbf{R}_0(\mathbf{r})).
 \end{aligned}
 \tag{2.1}$$

In the spirit of the quasiadiabatic propagator reviewed in the next section, our reference configuration $\mathbf{R}_0(\mathbf{r})$ is chosen to minimize the overall potential energy at each value of the x and z coordinates of hydrogen. The first derivative terms in the above equation vanish. The parameterized potential with all bath degrees of freedom relaxed with respect to each location of the hydrogen atom is shown in Fig. 2(a). This potential is further simplified via a quadratic expansion in the z coordinate along the one-dimensional path $z_H = g(x_H)/m_H\omega_\perp^2$ which minimizes the energy for a fixed value of x_H . With this expansion, the potential of the reference configuration takes the form

$$\begin{aligned}
 V(\mathbf{r}, \mathbf{R}_0(\mathbf{r})) \approx & V_{2d}(x_H, z_H) \\
 \equiv & V_0(x_H) \\
 & + \frac{1}{2} m_H \omega_\perp^2(x_H) \left(z_H - \frac{g(x_H)}{m_H \omega_\perp^2(x_H)} \right)^2,
 \end{aligned}
 \tag{2.2a}$$

where

$$V_0(x_H) = V(x_H, g(x_H), \mathbf{R}_0(x_H, g(x_H)))
 \tag{2.2b}$$

and

$$m_H \omega_{z_H}^2(x_H) \equiv \frac{\partial^2}{\partial z_H^2} V(\mathbf{r}, \mathbf{R}_0(\mathbf{r})) \Big|_{r=(x_H, g(x_H))}
 \tag{2.2c}$$

is the (variable) force constant of the hydrogen atom in the direction perpendicular to the line connecting two stable minima. For a given value of the system coordinate we calculate the one-dimensional potential V_0 using a ninth order polynomial interpolation, allowing 56 silicon atoms as well as the y and z coordinates of hydrogen to relax. The potential V_0 along the one-dimensional path $z_H = g(x_H)/m_H\omega_\perp^2$ is illustrated in Fig. 3(a). Herrero and Ramirez attribute the kinks to the inadequacy of the parameterized potential energy in the multidimensional region connecting the two minima. Such limitations are more pronounced in empirical potentials for solids with considerable lattice relaxation accompanying impurity motion. With the above approximation the lattice-independent term of the potential becomes a function of only the x of the hydrogen coordinate, which we designate as the system coordinate s . For simplicity the z coordinate of hydrogen is denoted as q .

The frequency ω_\perp associated with the z coordinate of the hydrogen atom varies by as much as a factor of four along the minimum energy valley $q = g(s)/m_H\omega_\perp^2$, while most of the remaining modes change by less than 10% from the B site to the saddle point region, the highest deviation arising from the mode associated with the y coordinate of hydrogen which undergoes a 20% variation. To simplify the

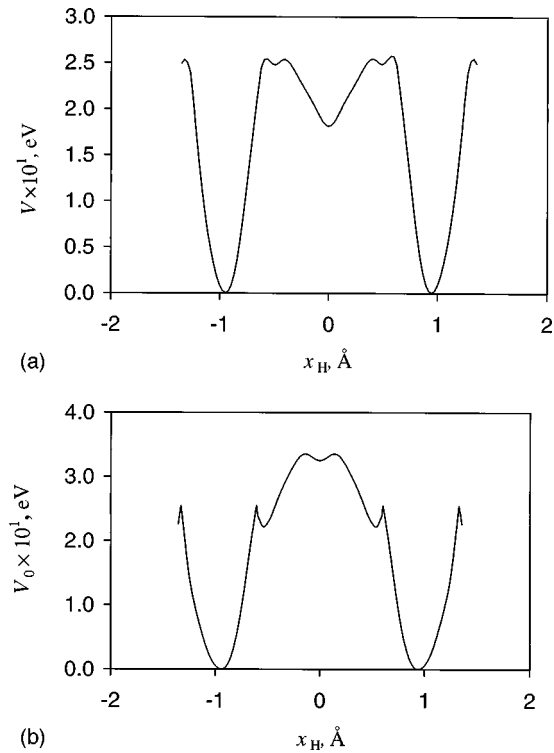


FIG. 3. (a) Potential energy surface along the minimum energy path (the first term in Eq. (2.2)) as a function of the x coordinate of the hydrogen atom. The P site corresponds to $x_H=0$. (b) Potential renormalized by the addition of the impurity's zero point energy along the z direction (see Eq. (2.2)) as a function of the x coordinate of hydrogen.

calculation we assume the modes and the corresponding force constants of the oscillators associated with the motion of the silicon lattice and the y coordinate of the hydrogen atom are throughout the dynamical process the same as those of the P site which corresponds to the system coordinate $s = s_P$. Evaluating the reference configuration through lowest order in the deviation from the one-dimensional minimum energy path $q = g(s)$ makes \mathbf{R}_0 a function of the system coordinate alone. With these assumptions the potential describing the bath degrees of freedom takes the form

$$\frac{1}{2} (\mathbf{R} - \mathbf{R}_0(s)) \cdot \mathbf{K} \cdot (\mathbf{R} - \mathbf{R}_0(s)),
 \tag{2.3a}$$

where \mathbf{K} is the force constant matrix at the P site,

$$\mathbf{K} \equiv \left. \frac{\partial^2 V(\mathbf{r}, \mathbf{R})}{\partial \mathbf{R} \partial \mathbf{R}'} \right|_{\mathbf{R}_0(s_P)}.
 \tag{2.3b}$$

The required second derivatives are calculated by finite difference. We note the above treatment neglects direct coupling between the z coordinate of hydrogen and the lattice displacements. Such coupling is deemed sufficiently weak.

It is useful to convert to the independent mode representation of Eq. (2.3a). For this purpose we define the transformation matrix \mathbf{U} and the normal mode coordinate vector \mathbf{Q} such that

$$\tilde{\mathbf{K}} \cdot \mathbf{U} = \mathbf{U} \cdot \mathbf{\Lambda}
 \tag{2.4}$$

and

$$\mathbf{R} - \mathbf{R}_0(s_P) = \mathbf{m}^{-1/2} \cdot \mathbf{U} \cdot \mathbf{Q}, \quad (2.5)$$

where $\tilde{\mathbf{K}} = \mathbf{m}^{-1/2} \cdot \mathbf{K} \cdot \mathbf{m}^{-1/2}$ is the force constant matrix in mass-weighted coordinates, Λ is the diagonal matrix of eigenvalues ω_i^2 and \mathbf{m} is a diagonal matrix that contains the atomic masses. Writing

$$\mathbf{R} - \mathbf{R}_0(s) = \mathbf{R}_0(s_P) - \mathbf{R}_0(s) + \mathbf{m}^{-1/2} \cdot \mathbf{U} \cdot \mathbf{Q} \quad (2.6)$$

leads to the following lattice normal mode representation of the hydrogen-silicon potential:

$$V(\mathbf{r}, \mathbf{R}) \approx V_{\text{rxn}}(s, q) + \sum_{i=1}^n \left(\frac{1}{2} \omega_i^2 Q_i^2 - f_i(s) Q_i \right), \quad (2.7)$$

where the reaction surface potential is given by the expression

$$V_{\text{rxn}}(s, q) \approx V_{2d}(s, q) + \frac{1}{2} (\mathbf{R}_0(s) - \mathbf{R}_0(s_P)) \cdot \mathbf{K} \cdot (\mathbf{R}_0(s) - \mathbf{R}_0(s_P)) \quad (2.8)$$

and

$$\mathbf{f}(s) = \mathbf{U}^T \cdot \mathbf{m}^{-1/2} \cdot \mathbf{K} \cdot (\mathbf{R}_0(s) - \mathbf{R}_0(s_P)) \quad (2.9)$$

is the coupling (force) vector. The forces $f_i(s)$ are a measure of the interaction between lattice and system (i.e., displacements in the lattice as the impurity moves) and the source of dissipation which leads to rate dynamics.

Due to its sizable variation along the reaction path, the frequency of the hydrogen impurity in the z direction cannot be treated as constant. By virtue of the quadratic expansion of the potential characterizing the reference configuration, Eq. (2.2), the z coordinate of the hydrogen atom acts as an additional bath oscillator whose frequency varies along the system coordinate. As a result, the potential of Eq. (2.8) takes the form

$$V_{\text{rxn}}(s, q) = V_{\text{eff}}(s) + \frac{1}{2} m_H \omega_{\perp}(s)^2 \left(q - \frac{g(s)}{m_H \omega_{\perp}(s)^2} \right)^2, \quad (2.10)$$

where the one-dimensional effective potential is

$$V_{\text{eff}}(s) \approx V_0(s) + \frac{1}{2} (\mathbf{R}_0(s) - \mathbf{R}_0(s_P)) \cdot \mathbf{K} \cdot (\mathbf{R}_0(s) - \mathbf{R}_0(s_P)). \quad (2.11)$$

Because the z_H degree of freedom couples only to the system coordinate s its effect on the dynamics can be captured via an appropriate influence functional which is obtainable in closed form. The latter is given explicitly in the Appendix. We note that the quadratic expansion of Eq. (2.2) is not essential to the methodology described in Sec. III, as the influence functional from a single anharmonic degree of freedom can still be calculated numerically.²⁶

It is interesting that a simplified one-dimensional treatment of the reaction surface can capture the main qualitative aspects of the diffusion process as well as providing insight into the unusual isotope effect that we observe. Taking advantage of the considerable mismatch between the local frequencies of the hydrogen atom in the x and z directions one can consider replacing the quadratically expanded reaction

surface by the potential $V_0(s)$ along the minimum energy path plus the adiabatic zero point energy in the z direction (see, for example, Refs. 27–29):

$$V_{\text{rxn}}(s, q) \rightarrow V_{\text{ad}}(s) \equiv V_{\text{eff}}(s) + \frac{1}{2} \hbar \omega_{\perp}(s). \quad (2.12)$$

Indeed, zero point vibration determines the effective barrier the hydrogen atom experiences, such that Eq. (2.12) gives the relevant potential to the extent that the motion is confined to a narrow valley surrounding the minimum energy path. Deviations from this picture, known as ‘‘corner cutting,’’ are responsible for quantitative differences in the results of this simplified treatment from those based on the full two-dimensional reaction surface.

The vibrationally adiabatic system potential energy, V_{ad} , is shown as a function of hydrogen’s x coordinate in Fig. 3(b). The apparent inversion of the potential energy in the metastable region is due to the added zero point energy of the hydrogen atom along the z direction. In the potential parameterization by Herrero and Ramirez, the frequency of the motion associated with the z coordinate initially lowers as the hydrogen moves away from the B site but rises as the metastable region is approached, leading to an increase of the barrier height in Fig. 3(b). This feature deviates from the results of Van de Walle *et al.*¹² in which the distance between the impurity and vertex silicon atom increases as the impurity moves from the B site to the region between the C and T sites. The resultant energy barrier we calculate is 0.34 eV for the zeroth order system Hamiltonian. It is important to remember, due to the adiabatic treatment, the barrier for deuterium is ~ 0.03 eV lower than the barrier for hydrogen diffusion. The value for the activation barrier is above the density functional theory value of 0.2 eV obtained by Van de Walle¹² and below that inferred from the high temperature experiments of Van Wieringen and Warmoltz.¹ Given the wide variance between experiment and theory regarding barriers we consider this value acceptable, in particular since the overall qualitative aspects of the hydrogen/deuterium dynamics process are of the utmost concern. The parameterized potential of Herrero and Ramirez captures the relevant potential features adequately.

III. RATE METHODOLOGY

With the exception of very low temperatures, impurity diffusion in solids is an incoherent process involving jumps between stable sites. In this regime the diffusion process is described by a rate equation. Below we focus at intermediate temperatures dominated by incoherent hops to neighboring potential minima. Effects of multiple hops become significant at high temperatures and have been the subject of other studies.⁹

The calculated rate constant corresponds to one-dimensional motion. To convert to diffusivity D , the rate constant k is multiplied by areal dimension A , in this case length of path squared, a symmetry factor w due to six equivalent B sites to which hydrogen can travel, and divided by twice the dimensionality $d=3$ of the problem,³⁰

$$D = k \frac{wA}{2d}. \quad (3.1)$$

It is useful to reference the rate with respect to classical transition state theory³¹ (TST), which involves the ratio of the partition function for the stable modes at the barrier top to that of the reactant configuration. With the two-dimensional treatment of the reaction surface the TST expression takes the form

$$k_{\text{TST}} = \frac{Z^{-1}}{2\pi\beta^2\omega_{\perp}^+} e^{-\beta E_b}, \quad (3.2a)$$

where Z is the classical partition function of the reactant well. Using the harmonic approximation to the reactant partition function, Eq. (3.2a) becomes

$$k_{\text{TST}} = \frac{\omega_0}{2\pi} \frac{\omega_{\perp}^0}{\omega_{\perp}^+} e^{-\beta E_b}. \quad (3.2b)$$

In the above equations $\beta = 1/k_B T$ is the inverse temperature in units of the Boltzmann constant, ω_0 is the frequency of the system potential at the stable point, ω_{\perp}^0 and ω_{\perp}^+ are the frequencies at the reactant minimum and (inverted) barrier top, respectively, and E_b is the barrier height of the two-dimensional potential defined in Eq. (2.2), which is the same as the barrier height of V_0 . Here the effects of variable frequency in the z coordinate enter through the ratio of frequencies at the two sites. In the results presented in the next section the reaction rate is referenced with respect to the more accurate TST expression, Eq. (3.2a), which is evaluated numerically. In the context of the simplified one-dimensional approximation to the z coordinate of hydrogen the TST expression reads

$$k_{\text{TST}}^{\text{ad}} = \frac{\omega_0}{2\pi} e^{-\beta E_b^{\text{ad}}}. \quad (3.2c)$$

In that case all effects due to the varying frequency of hydrogen enter through the modified energy barrier E_b^{ad} of the potential given by Eq. (2.12). The contribution of dynamical and/or quantum mechanical effects is conveyed through the transmission coefficient κ which is defined as the ratio of the reaction rate divided by its appropriate classical TST value.

Rigorous calculations of the rate constant require following the dynamics by classical or quantum mechanical methods. This task is most efficiently accomplished by evaluating the reactive flux that crosses a fictitious dividing surface separating reactants from products. The main advantage of the reactive flux formalism is that one need not follow the reaction from start to finish but only for a representative ‘‘plateau’’ time t_p . The system is placed at or near the saddle point of the potential surface with initial conditions selected from a statistical distribution and the ensuing dynamics followed for the time t_p chosen long compared to the molecular time scales of the systems but generally much shorter than the time required for transformation to products. The use of an equilibrium correlation function to infer the reaction rate rests on Onsager’s ‘‘regression hypothesis.’’³²

In the present case, where the potential surfaces exhibit a shallow minimum rather than a true saddle point at the midpoint between stable minima, placing the dividing surface at that point decreases the efficiency of the classical calculation as trajectories can be trapped there for considerable time

lengths. For this reason it is best to place the dividing surface at a saddle point in the classical calculation of the rate. If the dynamics is treated quantum mechanically, zero point energy effects prevent such trapping, while faster convergence of the path integral is observed when the dividing surface is placed at the P site.

A. Classical rate calculation

The transition state approximation ignores the possibility for recrossings of the dividing surface and therefore can only overestimate the rate within the framework of classical mechanics. Classical dynamical effects are captured in the reactive flux expression for the classical rate k_{cl} , which gives the transmission factor in the form³³

$$\kappa_{\text{cl}} \equiv \frac{k_{\text{cl}}}{k_{\text{TST}}} = \lim_{t \rightarrow t_p} (\langle \theta(x(t)) \rangle_+ - \langle \theta(x(t)) \rangle_-). \quad (3.3)$$

Here θ is the conventional step function. In the above expression the transmission factor is obtained as the difference between the fraction of initially reactive and non-reactive trajectories which end in the product region at time t .

We have calculated the classical transmission coefficient using Monte Carlo molecular dynamics; in particular, we followed a scheme developed by Zhang *et al.*³⁴ utilizing the Boltzmann operator of the system-bath Hamiltonian at the dividing surface as the sampling function.

We note that at the highest temperatures considered, where the rate is high, the classical correlation function exhibits early exponential decay rather than a well-defined plateau. In these cases we include a small correction factor to the rate given by the reactive flux formalism via the modification

$$Z^{-1} \int_0^t C_f(t') dt' = k \exp(-2kt). \quad (3.4)$$

B. Path integral methodology

Yamamoto,³⁵ as well as Miller and coworkers,^{36,37} have presented fully quantum mechanical expressions for determining reaction rates by calculating flux correlation functions. Here we adopt the formalism of Miller, Schwartz and Tromp,^{36,37} which expresses the rate constant in terms of the time integral of a flux correlation function,

$$k = Z^{-1} \int_0^{t_p} C_f(t) dt, \quad (3.5)$$

where the correlation function is defined as

$$C_f(t) = \text{Tr}(F e^{iHt_c^*/\hbar} F e^{-iHt_c/\hbar}). \quad (3.6)$$

In the last equation H is the Hamiltonian that characterizes the reaction and F is the symmetrized flux operator,

$$F = \frac{1}{2m_H} [p_s \delta(s - s_0) + \delta(s - s_0) p_s], \quad (3.7)$$

which measures the quantum mechanical reactive flux through a dividing surface that intersects the reaction coor-

dinate s at a point s_0 and which separates reactants from products. Finally, $t_c = t - i\hbar\beta/2$ is a complex time that arises from combining the time evolution operator with the Boltzmann operator. Eq. (3.5) is the starting point for numerous rigorous or approximate calculations of quantum mechanical rate constants.

Using the system-bath Hamiltonian developed in the last section, the starting point for our calculation of the quantum mechanical flux correlation function is Feynman's path integral formulation of quantum mechanics.^{38,39} Approximating the derivatives in Eq. (3.7) using finite difference the expression for the flux correlation function is brought into the form²³

$$C_f(t) = \frac{\hbar^2}{2m_H^2 s_{FD}^2} \text{Re}[K(s_{FD}, s_{FD}, 0, 0; t_c) - K(0, s_{FD}, 0, s_{FD}; t_c) + K(0, 0, 0, s_{FD}; t_c) - K(s_{FD}, 0, 0, 0; t_c)], \quad (3.8)$$

where s_{FD} is a system coordinate point chosen sufficiently close to the dividing surface to approximate derivatives and

$$K(s, s', s'', s'''; t_c) = \int dq \int d\mathbf{Q} \langle q | \langle \mathbf{Q} | \langle s''' | e^{iHt_c/\hbar} | s'' \rangle \times \langle s' | e^{-iHt_c/\hbar} | s \rangle | \mathbf{Q} \rangle | q \rangle. \quad (3.9)$$

Until recently, evaluation of path integral expressions involving real time propagators was generally unstable due to phase cancellation.⁴⁰ We have been able to obtain converged results using the quasiadiabatic propagator path integral (QUAPI) methodology for rate constants developed recently in our group.^{22,23} This employs a one-dimensional adiabatic reference to partition the time evolution operator. The reference Hamiltonian H_0 is constructed from the Cartesian kinetic energy of the system plus the potential along the one-dimensional adiabatic path which minimizes the total potential energy at fixed values of the system coordinate.²² This path is specified by the relations

$$Q_i = \frac{f_i(s)}{\omega_i^2}, \quad q = \frac{g(s)}{m_H \omega_\perp^2}. \quad (3.10)$$

The resulting reference Hamiltonian takes the form

$$H_0 = \frac{p_s^2}{2m_H} + V_{\text{eff}}(s) - \sum_{i=1}^n \frac{f_i(s)^2}{2\omega_i^2}. \quad (3.11a)$$

Notice that by virtue of Eqs. (2.4) and (2.9) we have

$$\sum_{i=1}^n \frac{f_i(s)^2}{2\omega_i^2} = \frac{1}{2} \mathbf{f}(s) \cdot \Lambda^{-1} \cdot \mathbf{f}(s) = \frac{1}{2} (\mathbf{R}_0(s) - \mathbf{R}_0(s_P)) \cdot \mathbf{K} \cdot (\mathbf{R}_0(s) - \mathbf{R}_0(s_P)) \quad (3.11b)$$

and thus the last term in Eq. (3.11a) cancels the terms added to Eq. (2.8) via the system-bath decomposition. As a result, the reference Hamiltonian is simply

$$H_0 = \frac{p_s^2}{2m_H} + V_0(s). \quad (3.12)$$

Similar relations hold for the simplified one-dimensional treatment but the potential of Eq. (3.12) is modified in that case to include the adiabatic zero point energy.

Next, the time evolution operator for a complex time increment Δt_c is split symmetrically as the product

$$\begin{aligned} \exp(-iH\Delta t_c/\hbar) &\approx \exp(-i(H-H_0)\Delta t_c/2\hbar) \\ &\times \exp(-iH_0\Delta t_c/\hbar) \\ &\times \exp(-i(H-H_0)\Delta t_c/2\hbar) \end{aligned} \quad (3.13a)$$

which can be evaluated in the coordinate representation to give the quasi-adiabatic approximation to the short time propagator. Use of the latter to evaluate the complex time evolution operators in Eq. (3.9) leads to the following QUAPI representation of the terms entering the expression for the flux correlation function, Eq. (3.8).²³

$$\begin{aligned} &K(s_1, s_{N+1}, s_{N+2}, s_{2N+2}; t_c) \\ &= \int_{-\infty}^{\infty} ds_2 \cdots \int_{-\infty}^{\infty} ds_N \int_{-\infty}^{\infty} ds_{N+3} \cdots \\ &\int_{-\infty}^{\infty} ds_{2N+1} \prod_{k=N+3}^{2N+2} \langle s_k | e^{iH_0\Delta t_c^*/\hbar} | s_{k-1} \rangle \\ &\times \prod_{k=2}^{N+1} \langle s_k | e^{-iH_0\Delta t_c/\hbar} | s_{k-1} \rangle \\ &\times F(s_1, s_2, \dots, s_N, s_{N+1}, s_{N+2}, \dots, s_{2N+2}). \end{aligned} \quad (3.13b)$$

Here $\Delta t_c \equiv t_c/N$ is a complex time step and F is an influence functional that arises from integrating out the bath. As mentioned in Sec. II, a modified influence functional is required to include the effects of the time dependent oscillator arising from the variable frequency treatment of the reaction surface:

$$F = F_{\text{harm}}(\{\omega_i, f_{ij}\}) F_{\text{anharm}}(\omega_\perp(s), g(s)). \quad (3.14)$$

The first component of this expression, the harmonic influence functional, was given explicitly in Ref. 23. The second factor is given in the Appendix.

The propagators involving the one-dimensional adiabatic reference H_0 are evaluated exactly using basis set methods, such that the only approximation entering Eq. (3.13) is due to the factorization of the propagator into parts involving non-commuting operators. This factorization becomes exact in the limit of a high-frequency bath. For finite frequency bath degrees of freedom the error introduced is proportional to the nonadiabaticity of the Hamiltonian and the quasi-adiabatic propagator becomes exact only in the limit of vanishing time step. Thus, the role of the influence functional in the quasi-adiabatic propagator path integral, Eq. (3.13), is to include multidimensional nonadiabatic corrections to the exact dynamics along the adiabatic path; these corrections become more accurate as the time slicing of the path integral becomes finer. Compared to conventional schemes for splitting the time-evolution operator which employ the bare kinetic energy as the reference, the QUAPI offers the advantage of convergence with much larger time steps.

The $(2N-2)$ -dimensional integral in the QUAPI representation of the flux correlation function are evaluated via a

combination of quadrature and Monte Carlo techniques. At higher temperatures the oscillatory character of the integrand necessitates the use of quadrature methods. Multidimensional integration is made feasible via the use of system-specific discrete variable representations⁴¹ (DVR) of the influence functional.²⁴ For this purpose the system coordinate operator s is diagonalized in the basis of eigenstates of the reference Hamiltonian H_0 , generating quasi-discrete position states with eigenvalues that form the DVR grid. As the temperature is lowered, more time slices are necessary for accurate discretization of the path integral, rendering multidimensional quadrature methods impractical. Fortunately, the stronger damping associated with lower temperature leads to smoother behavior of the integrand, making Monte Carlo schemes applicable.²³

At temperatures above 400 K the calculations presented in the next section converged with $N=3$ or 4 and employed multidimensional quadrature with 16 and 32 DVR points per integral dimension for H and D respectively. In this temperature range most quantum paths contributing to the flux correlation function are confined in the vicinity of the dividing surface. For this reason several points near the edges of the DVR grid can be neglected without significantly degrading the accuracy of the results. For hydrogen, with the present parameters we were able to reach convergence by treating explicitly a subset of only four DVR points closest to the dividing surface, leading to significant acceleration of the path integral calculations.

At or below room temperature a finer discretization of the time contour was necessary, with $N \leq 14$. The resulting integrals were evaluated via a variant of the Monte Carlo methodology developed by Topaler and Makri.²³ Enhanced efficiency was achieved by performing the Monte Carlo random walk on a multidimensional DVR grid of at most 64 points per dimension. Typically, the results shown in the next section were obtained with $10^5 - 10^6$ Monte Carlo points per integration variable.

Finally, the reactant partition function Z is calculated using the above methods except the time contour is solely imaginary.

IV. RESULTS

In this section we present our path integral results for the diffusion rate constant of hydrogen impurities in crystalline silicon. In order to deduce the role of quantum mechanical tunneling to the kinetics of hydrogen diffusion we compare the path integral results with those given by classical rate theory. We emphasize that the validity of our conclusions is intimately connected to the accuracy of the potential surface employed in the calculations, and the behaviors emerging from our work are to be understood primarily as qualitative trends.

Figure 4 shows the quantum mechanical reactive flux as a function of time at the temperatures $T=850$, 298 and 200 K as obtained via the procedure described in Secs. II and III employing explicit treatment of the hydrogen z coordinate dynamics. Significant recurrences are observed at the higher temperatures, which occur as the quantum reactive flux re-

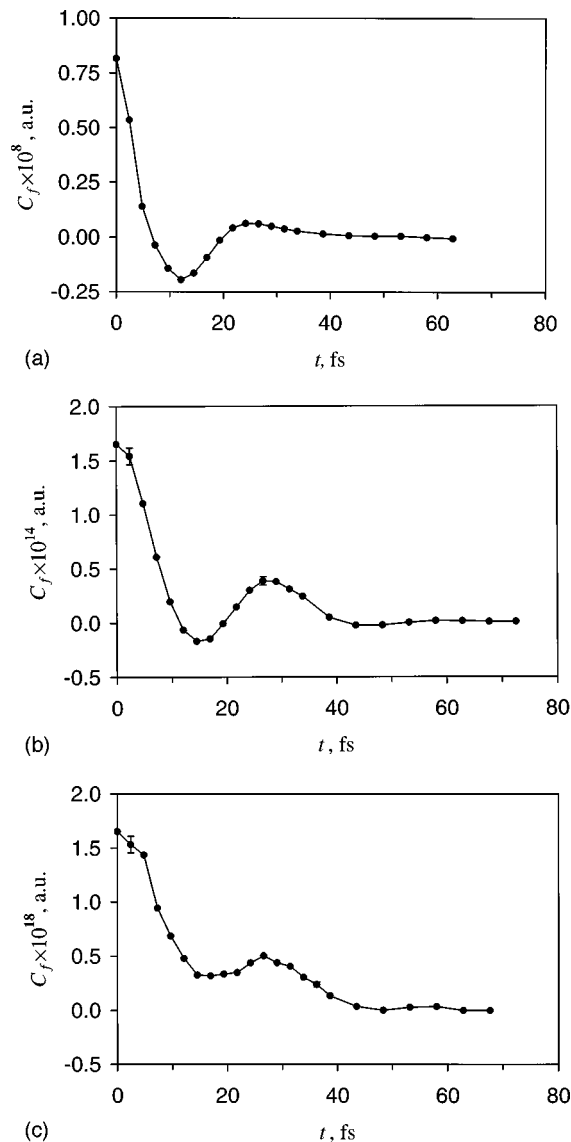


FIG. 4. Quantum flux correlation function at different temperatures calculated via explicit treatment of the hydrogen z mode. (a) $T=850$ K, (b) $T=298$ K and (c) $T=200$ K. The error bars correspond to one standard deviation of the Monte Carlo results and are representative of the errors at shorter and longer times.

crosses the dividing surface. These recrossings persist even at the lowest temperatures considered, although their magnitude decreases with decreasing temperature.

The classical and quantum mechanical diffusion rates for hydrogen are shown in Fig. 5 and compared to the classical TST estimate. These results are also given in Table I in terms of classical and quantum transmission coefficients expressed with respect to the appropriate two-dimensional or simplified adiabatic TST rate, Eq. (3.2b) or (3.2c), respectively. The rate is seen to vary by nearly ten orders of magnitude over the temperature range considered. The classical transmission factor is considerably smaller than unity. By rescaling the system-bath coupling coefficients we have verified that the process corresponds to the spatial diffusion (overdamped) Kramers regime.⁴²

Quantum tunneling effects are quite significant in this system, leading to a quantum transmission coefficient that

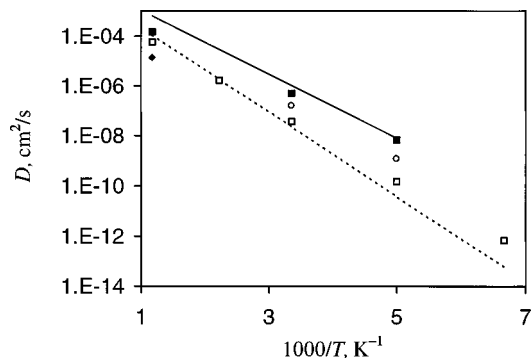


FIG. 5. Hydrogen diffusion rate as a function of inverse temperature. Solid line: transition state theory estimate, Eq. (3.2b). Dashed line: transition state theory estimate for the one-dimensional adiabatic model. Solid Squares: path integral results with explicit treatment of the hydrogen z mode. Hollow squares: path integral results for the one-dimensional adiabatic model. Hollow circles: classical trajectory results employing the two-dimensional reaction surface. Solid diamond: Van Wieringen and Warmholtz result.

exceeds significantly the classical one below room temperature. Even at 298 K, tunneling effects are responsible for a threefold increase of the diffusion rate. However, no noticeable flattening of the diffusion rate curve is found in the temperature range considered. We conclude hydrogen diffusion in this regime is an activated process with significant tunneling corrections and the expected crossover to the tunneling regime takes place at a temperature below 150 K.

We have also calculated the diffusion rate of deuterium in the same host. The results of these calculations are shown and compared to those obtained in the case of hydrogen in Fig. 6 and in Table II. The most striking feature of these data are the *increase* of the quantum mechanical diffusion rate of deuterium relative to hydrogen at intermediate temperatures. In order to gain insight into the origin of this unusual effect, we present in Tables I and II results obtained via the simplified one-dimensional treatment of the impurity in which the dynamics along the z coordinate is included through its zero point energy which is added adiabatically to the system potential. The reverse isotope effect we observe is due to a decrease of the effective barrier height in the case of deuterium caused by the zero point energy of the impurity's z coordinate when the latter is included adiabatically along the

TABLE I. Classical and quantum mechanical diffusion rates for hydrogen at various temperatures. (a) Two-dimensional treatment of the quadratically expanded reaction surface. (b) One-dimensional adiabatic treatment of the impurity vibration in the z direction.

T (K)	$D_{\text{TST}}^{\text{H}}$ (cm^2/s)	$\kappa_{\text{cl}}^{\text{H}}$	$\kappa_{\text{qm}}^{\text{H}}$
(a)			
850	6.31E-4	0.22±9%	0.23
298	1.05E-6	0.16±6%	0.48±8%
200	8.17E-9	0.15±10%	0.82±23%
(b)			
850	1.12E-4	0.36±1%	0.52
450	1.91E-6	0.38±2%	0.90
298	2.33E-8	0.40±2%	1.57±5%
200	3.90E-11	0.39±1%	3.84±8%
150	6.00E-14	0.38±2%	11.39±14%

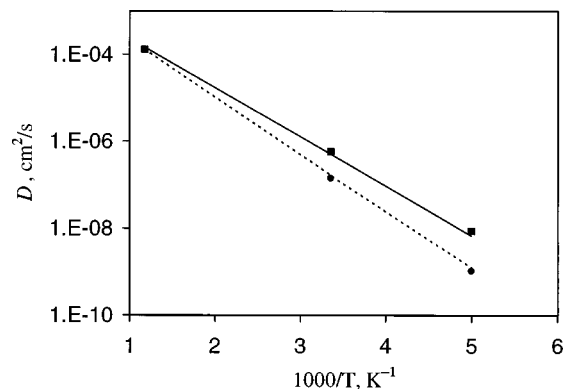


FIG. 6. Comparison of hydrogen and deuterium diffusion rates at different temperatures. Solid line: quantum mechanical diffusion rate of hydrogen. Dashed line: classical diffusion rate of hydrogen. Solid squares: quantum mechanical diffusion rate of deuterium. Solid circles: classical diffusion rate of deuterium.

reaction path. In the parameterized potential of Herrero and Ramirez the metastable state lies 1.28 Å above the vertex silicon compared to 1.47 Å for a hydrogen at a B site, resulting in a higher transverse frequency in the barrier region compared to that near a potential minimum, which increases the barrier height (cf. Eq. (2.2)). The larger mass of deuterium leads to a smaller increase of the potential in the barrier region and thus in a lower activation energy. This decrease of barrier height counteracts the conventional mass effect on tunneling, resulting in a small inverse isotope effect. The results of the one-dimensional approach are in qualitative agreement with those employing the two-dimensional reaction surface, although the simplified one-dimensional treatment appears to exaggerate the reverse isotope effect by ignoring dynamical effects, namely departures from the vibrationally adiabatic path, which oppose zero point energy conservation in the z direction, diminishing the difference of effective barriers. Finally, the classical calculations on the two-dimensional reaction surface ignore zero point effects and therefore exhibit the conventional isotope effect. A similar inverse isotope effect has been observed by Rick *et al.*⁴³ for the diffusion of hydrogen/deuterium on a palladium surface. If the variable frequency z mode of hydrogen/

TABLE II. Comparison of computed classical and quantum diffusivities for hydrogen and deuterium at various temperatures. (a) Two-dimensional treatment of the quadratically expanded reaction surface. (b) One-dimensional adiabatic treatment of the impurity vibration in the z direction.

T (K)	D_{qm}^{H}	$D_{\text{qm}}^{\text{H}}/D_{\text{cl}}^{\text{H}}$	D_{qm}^{D}	$D_{\text{qm}}^{\text{D}}/D_{\text{cl}}^{\text{D}}$
(a)				
850	1.48E-4	1.09±0.1	1.30E-4	1.01±0.06
298	5.03E-7±8%	3.05±0.52	5.84E-7±10%	4.14±0.62
200	6.7E-9±23%	5.40±1.8	8.7E-9E-9±28%	8.39±2.7
(b)				
850	5.89E-5	1.47±0.01	6.95E-5	1.66±0.01
450	1.72E-6	2.38±0.05	2.36E-6	2.1±0.04
298	3.66E-8±5%	3.93±0.03	5.34E-8±5%	2.60±0.18
200	1.50E-10±8%	9.8±0.9	2.55E-10±8%	4.15±0.4
150	6.83E-13±14%	29.9±4.8	1.34E-12±14%	8.34±1.3

deuterium is neglected completely the calculated diffusivities revert to the conventional isotope effect.

Although we are not aware of any experimental data for the diffusion rate of deuterium in crystalline silicon, a similar isotope effect has been observed by Stavola and Chang^{44,45} in the reorientation rate of hydrogen and deuterium in boron complexes embedded in silicon lattices. We note, however, that the inverse isotope effect borne by our calculations originates from delicate potential features and may be an artifact of parameterization of the hydrogen-silicon potential surface, in particular in the metastable region.

V. CONCLUDING REMARKS

We have calculated the diffusion rate of hydrogen and deuterium impurities in crystalline silicon using classical and quantum mechanical methods. The present study has been limited to single uncorrelated jumps which are dominant in the temperature range considered.

The motion of hydrogen impurities in crystalline silicon is strongly coupled to lattice vibrations. The strong frictional effects originating from these couplings lead to overdamped dynamics and cause a substantial decrease of the classical diffusion rate compared to the estimate of transition state theory.

The calculations presented in this paper reveal significant contributions of quantum mechanical phenomena to the site-to-site hopping rate of hydrogen in crystalline silicon. These phenomena manifest themselves primarily as tunneling corrections to the classical rate which persist even above room temperature. The crossover to tunneling dynamics occurs at a temperature below 150 K. In addition, zero point energy effects result in modification of the effective barrier height, leading to a weak reverse isotope effect. While the slope of the rate in the Arrhenius plot is smaller for deuterium in the activated regime, we expect the crossover to tunneling-dominated dynamics to occur at a lower temperature compared to that for hydrogen, below which the ordinary isotope effect should be observed. However, it remains to be verified that the potential features giving rise to these effects are not artifacts of the electronic structure calculation and/or the parameterization.

Contrary to our results, Herrero²⁰ does not observe a reverse isotope effect. However, the method employed in that work is approximate and hence may not capture the feature we observe due to the dynamics of the z coordinate relative to the x coordinate.

A reverse isotope effect has also been observed in experiments by Stavola *et al.*⁴⁴ These authors attribute this effect to larger zero-point motions of hydrogen resulting in greater lattice relaxations which in turn affect the rate. Doll

and co-workers have also reported a reverse isotope effect for hydrogen motion on the Pd(111) surface, in particular surface to subsurface transitions.⁴³ In that case, this effect is a consequence of the constricted quantum motions of coordinates orthogonal to the reaction coordinate leading to a higher free energy at the transition state relative to the reactant site for quantum motions which favors deuterium.

Recent experimental and theoretical studies have reported significant increase of silicon integrated circuit lifetimes due to decreased desorption rates when the silicon surface is passivated by deuterium rather than hydrogen.⁴⁶ While the hydrogen desorption process appears to proceed primarily via an excited electronic state, coupling to phonons and the quantum mechanical aspects of the process are likely to play a key role. Investigation of these effects via path integral methods will be a subject of future work.

ACKNOWLEDGMENTS

We are grateful to Carlos Herrero and Rafael Ramirez for preprints and to Maria Topaler for an early version of the rate program. We also thank the referee for thoughtful comments on the manuscript. This work has been supported by the National Science Foundation through a Young Investigator Award.

APPENDIX

Below we derive an expression for the influence functional arising from the variable frequency q oscillator (the z coordinate of the hydrogen atom) in the reactive flux correlation function. The influence functional takes the form²³

$$F_{\text{anharm}}(s_1, \dots, s_{2N+2}) = \text{Tr} e^{iH_{\perp}(s_{2N+2})\Delta t_c^*/2\hbar} \\ \times e^{iH_{\perp}(s_{2N+1})\Delta t_c^*/\hbar} \dots \\ e^{iH_{\perp}(s_{N+3})\Delta t_c^*/\hbar} e^{iH_{\perp}(s_{N+2})\Delta t_c^*/2\hbar} \\ \times e^{-iH_{\perp}(s_{N+1})\Delta t_c/2\hbar} e^{-iH_{\perp}(s_N)\Delta t_c/\hbar} \dots \\ e^{-iH_{\perp}(s_1)\Delta t_c/2\hbar}, \quad (\text{A1})$$

where H_{\perp} is the Hamiltonian for the hydrogen z coordinate obtained in Sec. II, which depends parametrically on the value of the system coordinate:

$$H_{\perp}(q, p_q; s) = \frac{p_q^2}{2m_H} + \frac{1}{2}m\omega_{\perp}^2(s) \left(q \frac{g(s)}{m_H\omega_{\perp}(s)^2} \right)^2. \quad (\text{A2})$$

By evaluating the trace in the coordinate representation and inserting complete sets of position states between each pair of exponentials Eq. (A1) is brought into the form of a $2N + 2$ -dimensional integral:

$$F_{\text{anharm}} = \int dq_1 \dots \int dq_{2N+2} \langle q_{2N+2} | e^{iH_{\perp}(s_{2N+2})\Delta t_c^*/2\hbar} | q_{2N+1} \rangle \langle q_{2N+1} | e^{iH_{\perp}(s_{2N+1})\Delta t_c^*/\hbar} | q_{N+2} \rangle \dots \\ \langle q_{N+2} | e^{iH_{\perp}(s_{N+2})\Delta t_c^*/2\hbar} | q_{N+1} \rangle \langle q_{N+1} | e^{-iH_{\perp}(s_{N+1})\Delta t_c/2\hbar} | q_N \rangle \dots \langle q_1 | e^{-iH_{\perp}(s_1)\Delta t_c/2\hbar} | q_{2N+2} \rangle. \quad (\text{A3})$$

Using the expression for the propagator of a displaced harmonic oscillator³⁹ and performing the Gaussian integral leads to the result

$$F_{\text{anharm}} = \pi^{N+1} (\det \mathbf{A})^{-1/2} R \exp(-\frac{1}{4} \mathbf{B}^T \cdot \mathbf{A}^{-1} \cdot \mathbf{B} + C). \quad (\text{A4})$$

Here \mathbf{A} is a $(2N+2) \times (2N+2)$ matrix with elements

$$A_{kk} = \theta_k \Omega_k + \theta_{k-1} \Omega_{k-1}, \quad k=1, \dots, 2N+2,$$

$$A_{k,k-1} = A_{k-1,k} = -\frac{im\omega_{\perp}(s_{k-1})}{2\hbar \sin\omega_{\perp}(s_{k-1})\Delta t_{k-1}} \theta_{k-1},$$

$$k=2, \dots, 2N+2, \quad (\text{A5})$$

$$A_{1,2N+2} = -\frac{im\omega_{\perp}(s_{2N+2})}{2\hbar \sin\omega_{\perp}(s_{2N+2})\Delta t_{2N+2}}.$$

\mathbf{B} is a $2N+2$ -dimensional vector with elements

$$B_k = \gamma_k \theta_k + \gamma_{k-1} \theta_{k-1}, \quad k=1, \dots, 2N+2 \quad (\text{A6})$$

and

$$C = 2 \sum_{k=1}^{2N+2} \lambda_k^2 \Omega_k \theta_k (\cos\omega_{\perp}(s_k) \Delta t_k). \quad (\text{A7})$$

The various quantities entering the above equations are

$$\theta_k = +1, \quad k=1, \dots, N-1,$$

$$k=0 \text{ or } N+1, \dots, 2N+2, \quad (\text{A8})$$

$$\Omega_k = \frac{im}{2\hbar} \omega_{\perp}(s_k) \cot(\omega_{\perp}(s_k) \Delta t_k), \quad (\text{A9})$$

$$\gamma_k = \frac{im\omega_{\perp}(s_k)\lambda_k}{\hbar \sin\omega_{\perp}(s_k)\Delta t_k} (1 - \cos\omega_{\perp}(s_k)\Delta t_k), \quad (\text{A10})$$

and

$$R = \prod_{k=1}^{2N+2} W_k, \quad (\text{A11})$$

where

$$\lambda_k = \frac{g(s_k)}{m_H \omega_{\perp}(s_k)^2}, \quad (\text{A12})$$

$$W_k = \left(\frac{m_H \omega_{\perp}(s_k)}{2\pi\hbar \sin\omega_{\perp}(s_k)\Delta t_k} \right)^{1/2}, \quad (\text{A13})$$

$$s_0 \equiv s_{2N+2}, \quad (\text{A14})$$

and

$$\Delta t_k = \begin{cases} \Delta t_c, & k=2, \dots, N \\ \Delta t_c^*, & k=N+3, \dots, 2N+1 \\ \Delta t_c/2, & k=1 \text{ or } N+1 \\ \Delta t_c^*/2, & k=N+2 \text{ or } 2N+2 \end{cases} \quad (\text{A15})$$

$$\Delta t_0 = \Delta t_{2N+2}.$$

The inverse and determinant are evaluated numerically via a linear decomposition method.²⁵ The result is applicable to any variable frequency harmonic oscillator.

¹A. Van Wieringen and N. Warmoltz, *Physica* **23**, 849 (1956).

²S. J. Pearton, W. Corbett, and M. Stavola, *Hydrogen in Crystalline Semiconductors* (Springer, Berlin, 1992).

³T. Ichimiya and A. Furuichi, *Int. J. Appl. Radiat. Isot.* **19**, 573 (1956).

⁴A. Fogro-Comperio, R. P. Love, and R. Schubert, *J. Electrochem. Soc.* **132**, 2006 (1985).

⁵A. J. Tavendale, A. A. Williams, D. Alexiev, and S. J. Pearton, *Mater. Res. Soc. Symp. Proc.* **104**, 285 (1988).

⁶S. J. Pearton, *J. Electron. Mater.* **14a**, 737 (1985).

⁷N. M. Johnson, D. K. Biegelsen, and M. D. Moyer, *Appl. Phys. Lett.* **40**, 882 (1982).

⁸F. Buda, G. L. Chiarotti, R. Car, and M. Parrinello, *Phys. Rev. Lett.* **63**, 294 (1989).

⁹G. Panzarini and L. Colombo, *Phys. Rev. Lett.* **73**, 1636 (1994).

¹⁰C. Langpape, S. Fabian, C. Klatt, and S. Kalbitzer, *Appl. Phys. A: Solids Surf.* **64**, 207 (1997).

¹¹P. Deak, L. C. Snyder, J. L. Lindstrom, J. W. Corbett, S. J. Pearton, and A. J. Tavendale, *Phys. Lett. A* **126**, 427 (1988).

¹²C. G. Van de Walle, P. J. H. Denteneer, Y. Bar-Yam, and S. T. Pantelides, *Phys. Rev. B* **39**, 10791 (1989).

¹³Y. V. Gorenkinskiy and N. N. Nevinnyi, *Sov. Tech. Phys. Lett.* **13**, 45 (1987).

¹⁴A. A. Bonapasta, A. Lapicciarella, N. Tomassini, and M. Capizzi, *Europhys. Lett.* **7**, 145 (1988).

¹⁵C. H. Seager and R. A. Anderson, *Am. Inst. of Phys.* **53**, 1181 (1988).

¹⁶D. E. Boucher and G. G. DeLeo, *Phys. Rev. B* **50**, 5247 (1994).

¹⁷R. Ramirez and C. P. Herrero, *Phys. Rev. Lett.* **73**, 126 (1994).

¹⁸C. P. Herrero and R. Ramirez, *Phys. Rev. B* **51**, 16761 (1995).

¹⁹C. P. Herrero and R. Ramirez, *Solid State Commun.* **97**, 319 (1996).

²⁰C. Herrero, *Phys. Rev. B* **55**, 9235 (1997).

²¹B. A. Ruf and W. H. Miller, *J. Chem. Soc. Faraday Trans. 2* **84**, 1523 (1988).

²²N. Makri, *Chem. Phys. Lett.* **193**, 435 (1992).

²³M. Topaler and N. Makri, *Chem. Phys. Lett.* **210**, 285 (1993).

²⁴M. Topaler and N. Makri, *Chem. Phys. Lett.* **210**, 448 (1993).

²⁵W. H. Press, S. A. Teukolsky, W. T. Vetterling, and B. P. Flannery, *Numerical Recipes*, 1st ed. (Cambridge University Press, Cambridge, 1989).

²⁶G. Ilk and N. Makri, *J. Chem. Phys.* **101**, 6708 (1994).

²⁷R. A. Marcus, *J. Chem. Phys.* **46**, 959 (1967).

²⁸D. G. Truhlar and A. Kuppermann, *J. Chem. Phys.* **56**, 2232 (1972).

²⁹R. A. Marcus and M. E. Coltrin, *J. Chem. Phys.* **67**, 2609 (1977).

³⁰S. W. Rick, D. L. Lynch, and J. D. Doll, *J. Chem. Phys.* **99**, 8183 (1993).

³¹K. J. Laidler, *Theories of Chemical Reaction Rates* (McGraw-Hill, New York, 1969).

³²L. Onsager, *Phys. Rev.* **38**, 2265 (1931).

³³B. J. Berne, in *Activated Barrier Crossing: Application in Physics, Chemistry and Biology*, edited by G. R. Fleming and P. Hanggi (World Scientific, Singapore, 1993), pp. 82–119.

³⁴Z. Zhang, K. Haug, and H. Metiu, *J. Chem. Phys.* **93**, 3614 (1990).

³⁵T. Yamamoto, *J. Chem. Phys.* **33**, 281 (1960).

³⁶W. H. Miller, *J. Chem. Phys.* **61**, 1823 (1974).

³⁷W. H. Miller, S. D. Schwartz, and J. W. Tromp, *J. Chem. Phys.* **79**, 4889 (1983).

³⁸R. P. Feynman, *Rev. Mod. Phys.* **20**, 367 (1948).

³⁹R. P. Feynman and A. R. Hibbs, *Quantum Mechanics and Path Integrals* (McGraw-Hill, New York, 1965).

⁴⁰N. Makri, *Comput. Phys. Commun.* **63**, 389 (1991).

⁴¹Z. Bacic and J. C. Light, *Annu. Rev. Phys. Chem.* **40**, 469 (1989).

⁴²H. A. Kramers, *Physica (Utrecht)* **7**, 284 (1940).

⁴³S. W. Rick, D. L. Lynch, and J. D. Doll, *J. Chem. Phys.* **99**, 8183 (1993).

⁴⁴M. Stavola and Y. M. Cheng, *Solid State Commun.* **93**, 431 (1995).

⁴⁵Y. M. Cheng and M. Stavola, *Phys. Rev. Lett.* **73**, 3419 (1994).

⁴⁶J. W. Lyding, K. Hess, and I. C. Kizilyalli, *Appl. Phys. Lett.* **69**, 2441 (1996).